Focused Experimental and Analytical Studies of the RBCC Rocket-Ejector Mode

M. Lehman, S. Pal, D. Schwer, J. D. Chen and R. J. Santoro
Department of Mechanical and Nuclear Engineering
The Pennsylvania State University
University Park, PA 16802

ABSTRACT

The rocket-ejector mode of a Rocket Based Combined Cycle Engine (RBCC) was studied through a joint experimental/analytical approach. A two-dimensional variable geometry rocket-ejector system with enhanced optical access was designed and fabricated for experimentation. The rocket-ejector system utilizes a single two-dimensional gaseous oxygen/gaseous hydrogen rocket as the ejector. To gain a systematic understanding of the rocket-ejector's internal fluid mechanic/combustion phenomena, experiments were conducted with both direct-connect and sea-level static configurations for a range of rocket operating conditions. Overall system performance was obtained through global measurements of wall static pressure profiles, heat flux profiles and engine thrust, whereas detailed mixing and combustion information was obtained through Raman spectroscopy measurements of major species (gaseous oxygen, hydrogen, nitrogen and water vapor). These experimental efforts were complamented by Computational Fluid Dynamic (CFD) flowfield analyses.

INTRODUCTION

Recent interest in low cost, reliable access to space has generated increased interest in advanced technology approaches to space transportation systems. A key to the success of such programs lies in the development of advanced propulsion systems capable of achieving the performance and operations goals required for the next generation of space vehicles. One extremely promising approach involves the combination of rocket and air-breathing engines into a rocket-based combined-cycle engine (RBCC). Although there are several design variations for the RBCC engine, the garnut of concepts includes four flight regimes, viz. rocket-ejector, ramjet, scramjet and all-rocket [1]. Of these four flight regimes, the rocket-ejector mode that encompasses the zero to roughly two Mach number range of the flight vehicle, is the least well understood. Studies of RBCC engine concepts are not new and studies dating back thirty years are well documented in the literature. However, studies focused on the rocket-ejector mode of the RBCC cycle are lacking.

The present investigation utilizes an integrated experimental and computation fluid dynamics (CFD) approach to examine critical rocket-ejector performance issues. The experimental phase of this program includes studying the mixing and combustion characteristics of the rocket-ejector system utilizing Raman spectroscopy in conjunction with heat flux, static pressure and thrust measurements. For this purpose, a two-dimensional variable geometry rocket-ejector system with optical access was designed and fabricated. Complementary CFD analyses were also conducted to provide further insight into the rocket-ejector mode of operation.

In this paper, the experiments and analysis conducted for a Diffusion and Afterburning (DAB) rocket-ejector configuration [2] are presented and discussed. The experimental setup and CFD analysis methodology are introduced first before the experimental/analytical results are presented and discussed. Finally, plans for future efforts are briefly discussed.

EXPERIMENTAL

The experimental configuration used for the rocket-ejector studies is based on the well known 1968 experimental rocket-ejector study of Odegaard and Stroup [3]. It is recognized that advancements of both proprietary and classified natures have been made in the last thirty years, however, this particular geometry was chosen as the baseline configuration because it represents the most comprehensive set of data available in the open literature. The scope of the current study is not to simply duplicate the experiments of Odegaard and Stroup, but to build on this study by bringing to bear advances made in both diagnostic and analytical techniques to document the flow characteristics of the rocket-ejector mode of the RBCC engine.

ROCKET-EJECTOR SETUP

A single rocket based optically accessible air augmented rocket-ejector system was designed and fabricated for the experiments. Schematics of the setup are shown in Fig. 1 for both direct-connect and Sea-level static (SLS)

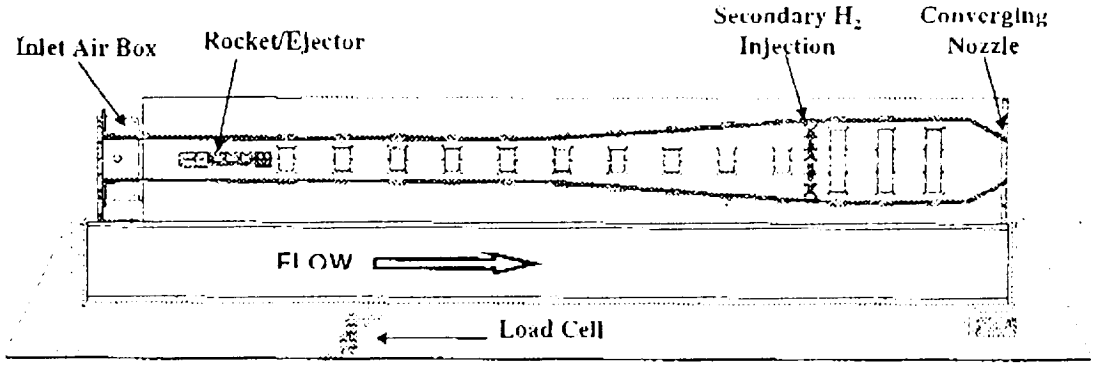

(a) Direct-connect configuration

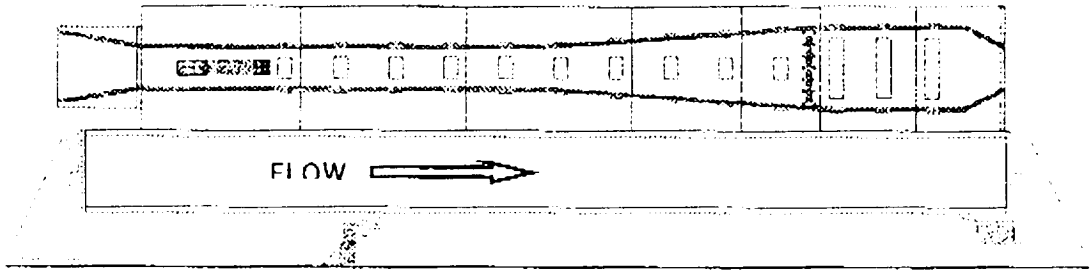

(b) Sea-level static configuration

Fig. 1. Rocket-ejector setups.

configurations. The design features a single two-dimensional gaseous oxygen (GO_2)/gaseous hydrogen (GH_2) rocket that is used as the ejector. A schematic of the rocket is shown in Fig. 2. The rocket-ejector system stresses modularity for studying the important effects of preferred nozzle primary area ratios, primary-secondary pressure matching and thermal choking. The two-dimensional design enables the easy change of the rocket-ejector's mixer length, diffuser length and angle, afterburner length and exit nozzle geometry. In addition, the entire length of the duct beyond the exit plane of the rocket nozzle is optically accessible which enables the application of non-intrusive laser-based diagnostics. The entire system is mounted on a load cell for thrust measurements and is equipped with multiple static pressure ports and heat flux gauges along the vertical and horizontal duct walls.

The compact rectangular cross-sectioned gaseous hydrogen/oxygen rocket shown in Fig. 2 was designed specifically for stoichiometric GO_2/GH_2 operation at 500 psia. The rocket injector body utilizes 6 shear coaxial elements in a horizontal array and is not actively cooled. The internal dimensions of the chamber section are 6 inches long, 3 inches wide and 0.5 inch tall. The nozzle reduces to a throat height of 0.1 inch and expands to a height of 0.6 inch. The rocket chamber and converging/diverging nozzle sections are both actively cooled with water during each firing.

The experimental results discussed in this paper were obtained for the fixed DAB rocket-ejector geometry shown in Fig. 1. Experiments were conducted for both direct-connect and SLS configurations. For the direct-connect experiments air was introduced into the system (see Fig. 1 (a)), whereas for the SLS configuration, a two-dimensional inlet was employed (see Fig. 1 (b)). The mixer and diffuser length are both 35 inches whereas the internal width of the duct is 3 inches. The internal height expands from 5 to 10 inches throughout the diffuser length, and the exit

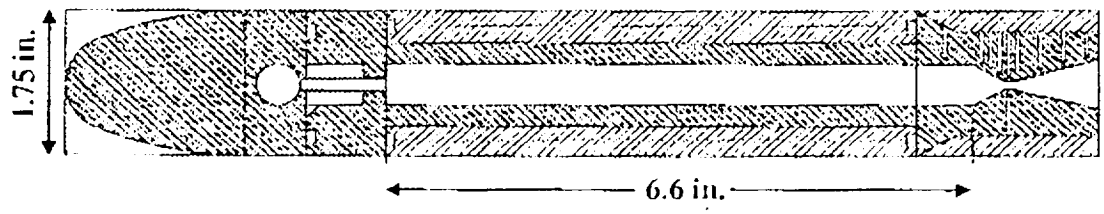

Fig. 2. Schematic of two-dimensional gaseous oxygen/gaseous hydrogenrocket chamber.

Table 1. Flow conditions.

	Direct-connect				SLS	
	Case 1	Case 2	Case 3	Case 4	Case 5	Case6
Rocket						
O/F	4	4	8	8	4	8
GO_2 Flowrate (lbm/s)	0.470	0.470	0.608	0.608	0.470	0.608
GH_2 Flowrate (lbm/s)	0.118	0.118	0.076	0.076	0.118	0 076
Chamber Pressure (psia)	500	500	500	500	500	500
Duct						
Air Flow (lbm/s)	1.575	2.016	1.575	2.016	*1.29**	*1.24**
GH_2 Flow in Afterburner (lbm/s)	0	0	0.046	0.059	0	0 046
Excess GH_2 in Rocket Exhaust (lbm/s)	0.06	0.06	0	0	0.06	0
GO_2 in Airflow (lbm/s)	0.368	0.47	0.368	0 47	*0.301*	*0.290*
O/F Between GO_2 in Air and GH_2 in Duct	6.25	8	8	8	*5.02*	*6.30*

* For SLS conditions, ejected airflow rate is measured. Items in *italics* were calculated after experiments.

nozzle of the air duct converges from 10 inches to an exit height of 5 inches. The single GO_2/GH_2 rocket was designed for optimum performance at an operation pressure of 500 psia at stoichiometric flow conditions.

ROCKET-EJECTOR OPERATING CONDITIONS

Six operating conditions were investigated, details of which are summarized in Table 1. These conditions include both stoichiometric rocket/afterburner and fuel-rich rocket/no afterburner operation for a fixed rocket chamber pressure of 500 psia. Results of earlier experiments conducted for a similar matrix of flow conditions but at a lower rocket chamber pressure of 200 psia can be found in Refs. 4 and 5. In Table 1, cases 1-4 are for the direct-connect configuration whereas cases 5-6 are for the SLS geometry. For cases 1, 2 and 5, the operating mixture ratio of the rocket was four. For these three cases, there was no downstream introduction of GH_2. The first two cases differ in the amount of air introduced into the system, whereas for the SLS case, air is ejected into the system. For case 1, the excess GH_2 in the rocket plume depletes the GO_2 in the air stream, whereas for case 2, the airflow is defined such that the GO_2 in the air can burn stoichiometrically with the excess GH_2 in the rocket exhaust. For cases 3, 4 and 6, the operating GO_2/GH_2 mixture ratio was stoichiometric. The first two conditions (cases 3 and 4) differ in the amount of introduced air, and therefore the bypass ratio which is defined as the ratio between the airflow and total propellant flow. For these two direct-connect cases, the afterburner was operational, with the amount of injected GH_2 set to burn stoichiometrically with the GO_2 in the air stream. The additional hydrogen was injected into the flowfield at the upstream end of the afterburner through a series of 0.1 in. diameter holes. Seven holes spaced 1 in. apart on each side of the duct provided cross-stream injection of hydrogen at this location. Finally, for the direct-connect experiments (cases 1-4), the introduced airflow simulated conditions of Mach 1 at 9400 ft and Mach 1.9 at 40,000 ft for a nominal 1000 psf dynamic pressure trajectory, whereas the use of an inlet allowed experimentation at SLS conditions (cases 5-6). These conditions are the same as those tested for the Odegaard and Stroup study [3].

It is noted that for the chosen rocket-ejector DAB geometry, viz. mixer, diffuser, afterburner and converging nozzle tandem, near-stoichiometric rocket operation with secondary combustion in the afterburner is thermodynamically more efficient. Therefore, the flow distribution for cases 3, 4 and 6 is expected to be more efficient than the remaining three cases. The experiments with the fuel-rich rocket, i.e. cases 1, 2 and 5, were conducted to a) provide design guidance for future Simultaneous Mixing and Combustion (SMC) strategies where thermal choking is employed and b) further the experimental data base for CFD code refinement.

RAMAN SPECTROSOCPY SETUP

The mixing and combustion processes within the rocket-ejector system were studied using spontaneous Raman spectroscopy. This technique has been utilized in the past at Penn State for measurements of major species concentrations and temperature in a rocket environment [6]. For the present experiments, the technique was implemented for line measurements of the major species, viz. GH_2, GO_2, gaseous nitrogen (GN_2) and water vapor (H_2O). The setup schematic is shown in Fig. 3. A frequency doubled Nd:YAG laser, λ=532 nm, was used as the excitation source. The laser beam was passed vertically through the air duct in a focused line. The laser operated at a short pulse length of approximately 12 ns and produced 750 mJ per pulse. This resulted in an energy flux that exceeded the damage threshold of the quartz windows used to pass the beam through the air duct. To overcome this limitation, the laser pulse was stretched by means of a beam splitter and pulse delay path length. This served to stretch the pulse to nearly 30 ns. After the beam had traveled along the pulse delay path, the laser beam was then directed vertically up to an elevated optical rail that redirected the beam over the top of the air duct. After the beam passed through a 1 m focusing lens, it was reflected down through the air duct by means of the previously mentioned

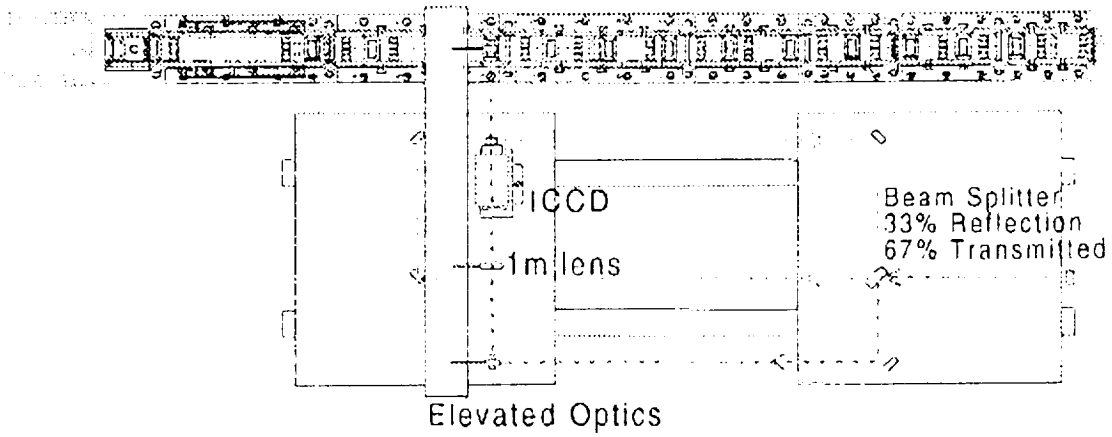

Fig. 3. Top view of Raman spectroscopy setup.

sealed quartz window. The focal point of the laser beam matched the centerline of the air duct and the side window. Through this window, the Raman signal was collected at 90° to the beam by an ICCD camera (12 bit dynamic range; EEV CCD chip, 576x384 pixels) using either an imaging spectrometer or species specific bandpass filters with a f/1.2 50 mm *f*/ Nikon lens. The spectrometer was used only at the first window location, 2.5 inches downstream from the rocket nozzle exit plane, and required 4x6 pixel binning for image analysis. Beyond the first window, species specific 10 nm bandpass filters were required due to their higher signal collection efficiency, and 4x4 pixel binning was used. For the wavelength of the laser used here (λ=532 nm), the peak wavelengths for the Stokes vibrational Q-branch Raman signals from CO_2, GH_2, GN_2 and H_2O are 580, 680, 607 and 660 nm, respectively [5,6]. For each firing, the collected Raman signal was then sent to a personal computer for storage and eventual analysis. The test duration was set for 4 seconds of steady state combustion. Within this timing sequence, each firing provided 15-20 instantaneous Raman images. The laser operated at 10 Hz, but the camera readout rate slowed acquisition to approximately 5 Hz. Images were then discarded or retained based on image quality. Images that had pixel saturation in any region were not included in the averaging process. The technique was applied for making species measurements at the first four window locations downstream of the rocket nozzle exit plane. The goal was to establish at what location the flow of the ejector was fully mixed with the air and at what location any excess GH_2 had been consumed.

CFD METHODOLOGY

An in-house CFD code, viz. Diagonalized Upwind Navier Stokes (DUNS) code capable of computing turbulent combustion flowfields typical of RBCC rocket-ejector flowfields was used. Since the description of the code [7,8] is beyond the scope of this paper, only the key salient features are described. The code has the capability to handle complex geometries through a general multi-blocking strategy for computing the preconditioned Navier Stokes equations for laminar and turbulent flowfields. The turbulence model is the two-equation, viz. q-ω, low Reynolds number model developed by Coakley [9]. The code employs the Alternating Direction Implicit (ADI) scheme [10] diagonalized using the procedure of Pulliam and Chaussee [11] to reduce CPU and computer storage requirements. The code uses a cell-centered, finite-volume approach and has the flexibility of modeling the convective terms as 1st-order upwind, 2nd order upwind, 3rd-order upwind-biased or 5th-order upwind-biased differencing. An option to invoke Total Variation Diminising (TVD) flux evaluations is available for the 2nd-order upwind and 3rd-order biased differencing in order to cleanly capture sharp gradients in the flowfield. The diffusive terms are modeled with 2nd-order central differencing. The DUNS code achieves time-accuracy through the use of a dual-time stepping procedure. This procedure enhances the robustness of the code especially for steady state problems for which reasonable initial solutions are not available.

The combustion model employed in the DUNS code is the 9-species, 18-step oxygen/hydrogen chemistry model. However, initial tests of the multi-step reaction mechanism revealed convergence difficulties and non-physical solutions. Based on these initial difficulties, initial computations reported in this paper were performed with a single-step reaction mechanism. This single step mechanism provides a convenient method of qualitatively adding heat to the flowfield based on the local presence of oxygen and hydrogen. The actual heat release was controlled by adjusting the heat of formation of water. The value of the heat of formation was determined in an iterative manner by using the CEA code [12] for equilibrium chemistry at the specified mixture fraction ratios and approximate flow conditions. The iterative procedure indicated that reducing the heat of formation of water by approximately 22% for the single-step reaction mechanism yielded temperatures comparable to CEA predictions.

RESULTS AND DISCUSSION

Global measurements in terms of axial static pressure profiles, wall heat flux profiles and engine thrust were made for all six cases listed in Table 1. Detailed measurements of the major species (gaseous O_2, H_2, H_2O and N_2) concentrations at various axial locations (window locations; please see Fig. 1) were made to characterize the mixing and combustion between the supersonic rocket exhaust and subsonic airstream for all the direct-connect configuration cases (cases 1-4) and the stoichiometric rocket/afterburner SLS case (case 6). For the SLS cases, the ejected airflow rate was inferred from high accuracy static pressure measurements in the inlet section. The ejected airflow rates for cases 5 and 6 are also tabulated (and highlighted) in Table 1.

In the following sections, these experimental results are presented and compared with complementary CFD flowfield predictions.

GLOBAL FLOWFIELD DESCRIPTION

Inspection of the CFD predictions for the SLS fuel-rich rocket/no afterburner case (case 5) provides a global qualitative description of the flowfield within the rocket-ejector system. The Mach number, temperature contours as well as both the hydrogen and oxygen mole fraction contours are shown in the four inset graphs of Fig. 4. For each inset graph, contour levels are shown for the entire rocket-ejector geometry as well as for the near rocket exhaust region. The Mach number contour plot shows the mixing of the supersonic hydrogen-rich rocket exhaust with the subsonic airstream in the mixer section of the rocket-ejector. The close-up Mach number contour plot shows that the flowfield in the nozzle expansion section is well behaved and the existence of a recirculation region in the lip area of the nozzle. The corresponding temperature contour plot indicates that the flow approaches near complete mixedness at the start of the diffuser section. The mole fraction plots of hydrogen and oxygen also indicate that combustion

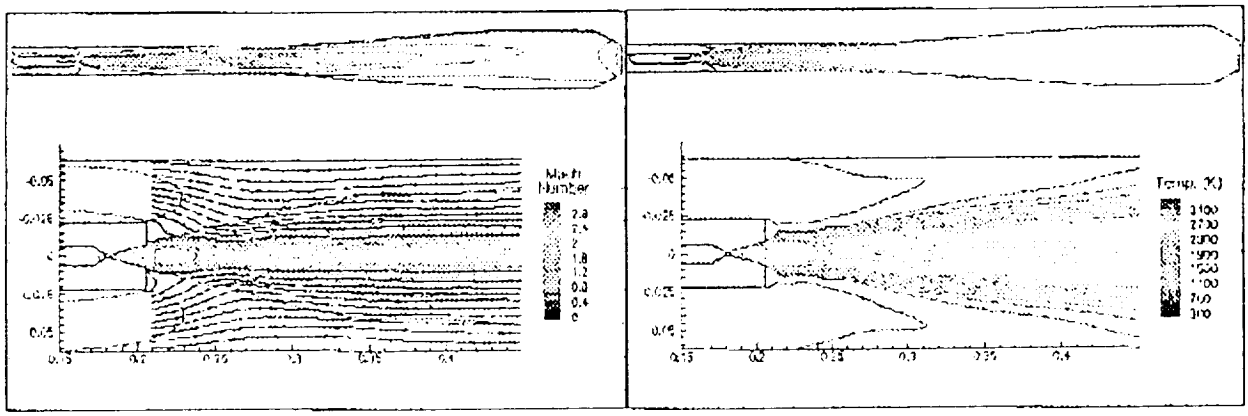

(a) Mach number contours

(b) Temperature contours

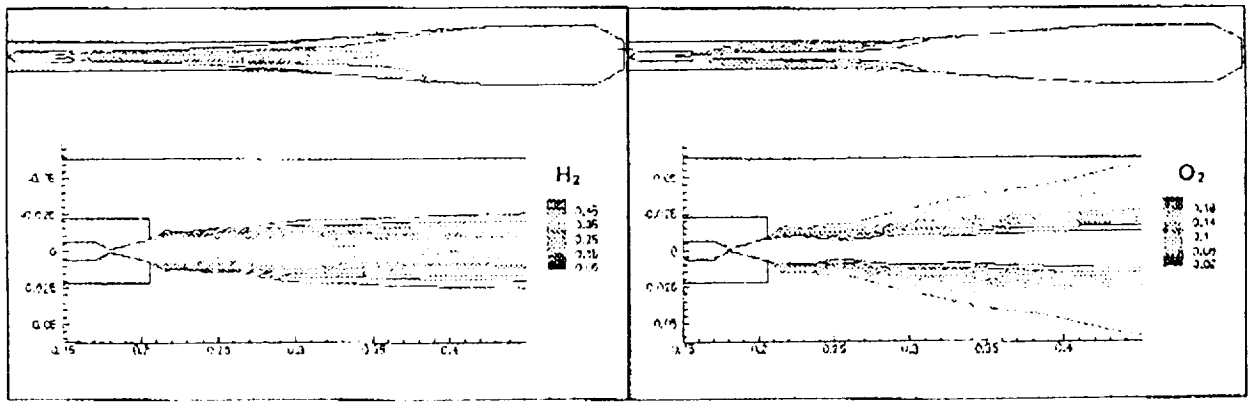

(c) H_2 mole fraction contours

(d) O_2 mole fraction contours

Fig. 4. CFD predictions for the fuel-rich rocket/no afterburner SLS case, (case 5, Table 1). For each inset graph, contours are shown for the entire flowfield as well as for the near rocket exhaust region. Please note that dimensions are in SI units(L=meter; T=Kelvin).

between the excess hydrogen in the rocket exhaust and oxygen in the airstream nears completion by the end of the mixer region. The CFD predictions for case 5 discussed here and for the other cases indicate qualitatively that the mixer length is "appropriate" for achieving complete mixing and combustion.

The CFD predictions for the SLS conditions were also integrated to estimate the airflow ejected by the rocket. For the flow conditions of case 5, the CFD calculations indicate that 1.15 lbm/s of air is ejected which compares reasonably well with the experimentally measured result of 1.29 lbm/s.

MIXING AND COMBUSTION RESULTS

Raman spectroscopy measurements of the major species in the flowfield were made at the window locations in the mixer section of the rocket-ejector setup for all the direct-connect cases and the stoichiometric rocket/afterburner SLS case. At each window location, multiple instantaneous measurements were made for each species. These measurements were then averaged and analyzed to obtain species concentration profiles for each species. Several authors [13-15] have reviewed the theory of Raman spectroscopy and its usefulness in making species and temperature measurements; therefore, only a brief description of the analysis will be given here. Eq. 1 shows how the Raman signal intensity relates to the individual species mole fractions and the overall gas temperature and pressure.

$$S_i = k_i f_i(T) \eta_i \tag{1}$$

S_i = Raman Signal Intensity
k_i = Signal Collection Constant
$f_i(T)$ = Bandwidth Factor
η_i = Species Number Density
In terms of species' mole fraction,

$$\chi_i = \frac{S_i}{f_i(T) k_i \left(\frac{P}{RT}\right)} \tag{2}$$

The signal collection constant, k_i, is obtained from cold flow measurements of pure species through the rocket body. With temperature and pressure equal to ambient conditions, the appropriate Raman signal was collected, mole fraction and $f_i(T)$ were set to unity, so then the sole unknown in Eq. 1 was k_i. This signal collection constant was then applied to the hot fire analysis. For hot fire conditions, the Raman signal was again collected, but species' mole fraction, the species' bandwidth factors and temperature were not known. The bandwidth factor term accounts for variation in the fraction of total scattered signal. It depends on spectral location, shape and bandwidth of the detection system. $f_i(T)$ was calculated from a polynomial curve fit theoretically determined [16] for the range of temperatures expected in these experiments, 300K-3500K. The final analysis then required an iteration based on temperature. The temperature was varied until the sum of the four species' mole fractions was unity, using Eq. 1 and the four bandwidth factor polynomials. This iteration was done for each of the vertical pixel locations in the Raman signal field of view in order to return corresponding temperature and mole fraction profiles within the duct.

The final results for two cases, viz. case 3 and 6, are shown in Figs. 5 and 6, respectively. Recall that both cases are for stoichiometric rocket operation with the afterburner on. Case 3 is for the direct-connect configuration whereas case 6 is for the SLS geometry. In both figures, the mole fractions of only nitrogen and water vapor are shown for clarity. Measurements were also made for hydrogen and oxygen but are not shown here. Inspection of the mole fraction plots of nitrogen and water vapor at the various axial measurement locations shows the mixing between the rocket exhaust and airstream. In both figures, the axial locations are indicated with respect to distance from the rocket nozzle exit plane. The axial locations non-dimensionalized with respect to both the rocket nozzle exit height, h, as well as the duct height, d, are also indicated. The nitrogen and water vapor mole fraction profiles for both cases 3 and 6 show that mixing is complete at or before the fourth axial measurement location (x=23.5 in.; x/h=39.2, x/d=4.7). Similar results (not shown here) for the fuel-rich rocket/no afterburner cases (1 and 2) show that all mixing and combustion phenomena are complete within the fifth axial measurement location (x=30.5 in.; x/h=50.8, x/d=6.1).

GLOBAL RESULTS

Global results in terms of axial static pressure profiles, wall heat flux and engine thrust were obtained for all the cases listed in Table 1. For each hot fire test, static pressure and heat flux measurements were also recorded. The static pressure values were recorded through 16 channels on both the side and top wall of the air duct. The values were acquired at 6 Hz and averaged over the steady state combustion period. The heat flux measurements were acquired at 200 Hz using multiple 0.5 in. diameter Gardon heat flux gauges. Measurements

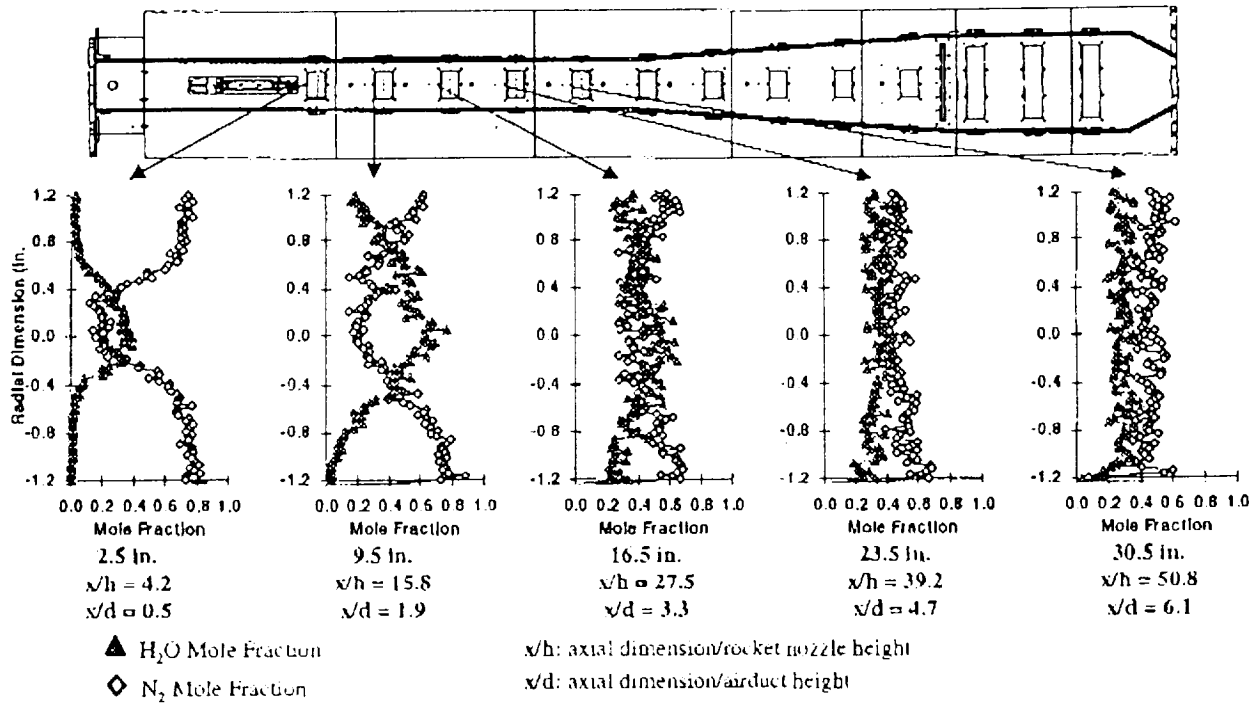

Fig. 5. Profiles of H_2O and N_2 mole fraction at five axial locations for the direct-connect configuration, stoichiometric rocket/afterburner operation (case 3, Table 1).

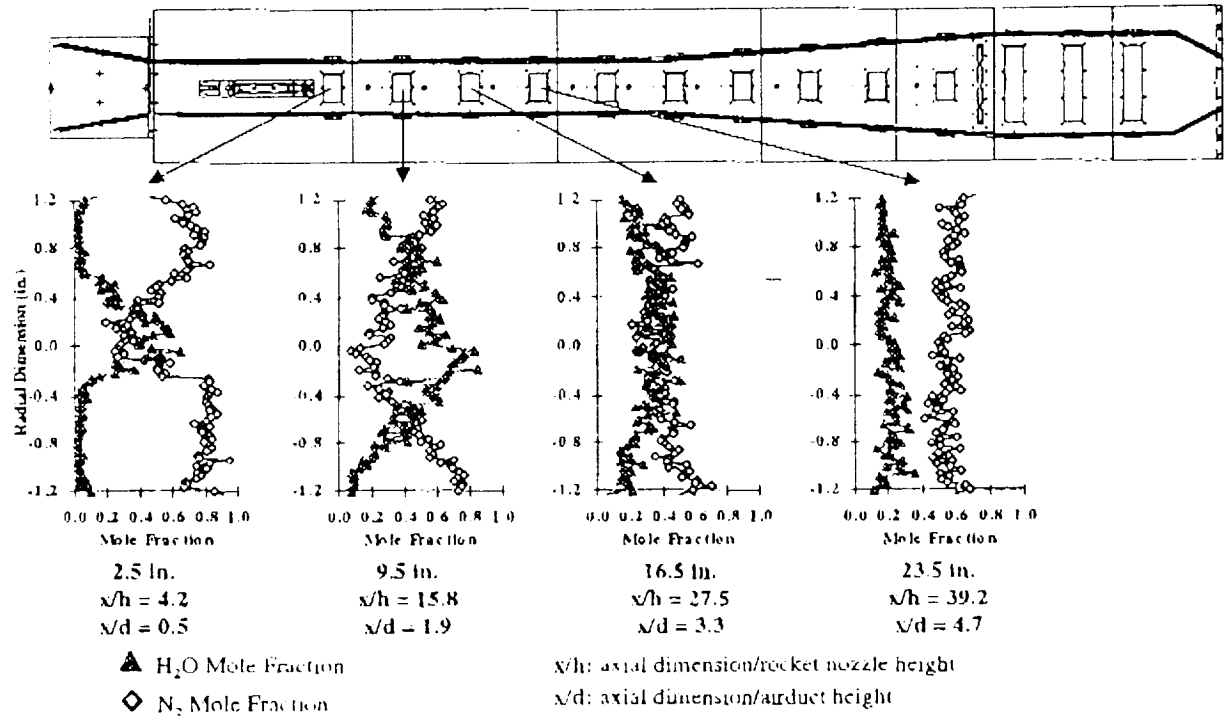

Fig. 6. Profiles of H_2O and N_2 mole fraction at four axial locations for the SLS configuration, stoichiometric rocket/afterburner operation (case 6, Table 1).

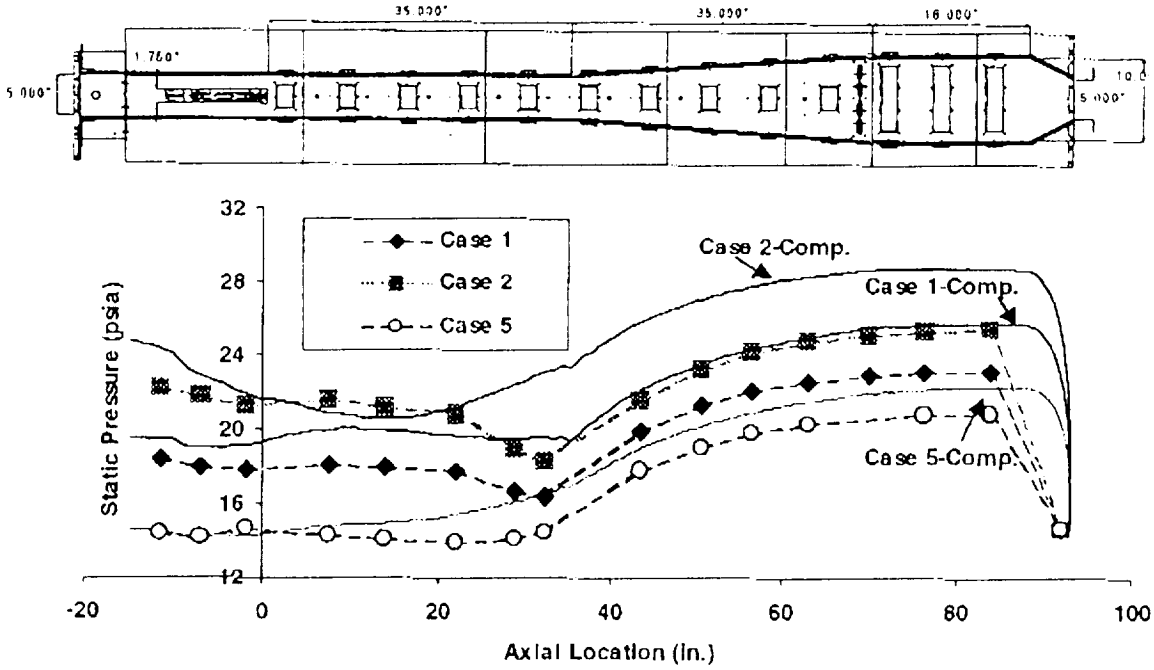

Fig. 7. Comparison of axial static pressure profiles between experimental results and CFD predictions. Results shown are for fuel-rich rocket operation for both direct-connect (cases 1 and 2) and SLS (case 5) configurations. Note that for the SLS condition there is an inlet for the rocket-ejector system.

were made along both the side and top walls for all cases in Table 1. A select set of these measurements are discussed in this sub-section.

Axial static pressure profiles within the duct for the fuel-rich rocket/no afterburner cases (cases 1, 2 and 5) are compared with the CFD code predictions in Fig 7. The experimental results for the fuel-rich rocket cases show a decrease in the static pressure in the mixer section resulting from combustion between the fuel in the rocket exhaust and the airstream. In the diffuser section, the static pressure increases until it reaches the second constant area section. Within this constant area section, the static pressure remains relatively constant. Finally, as expected, the flow accelerates in the converging nozzle, and consequently, the static pressure drops accordingly.

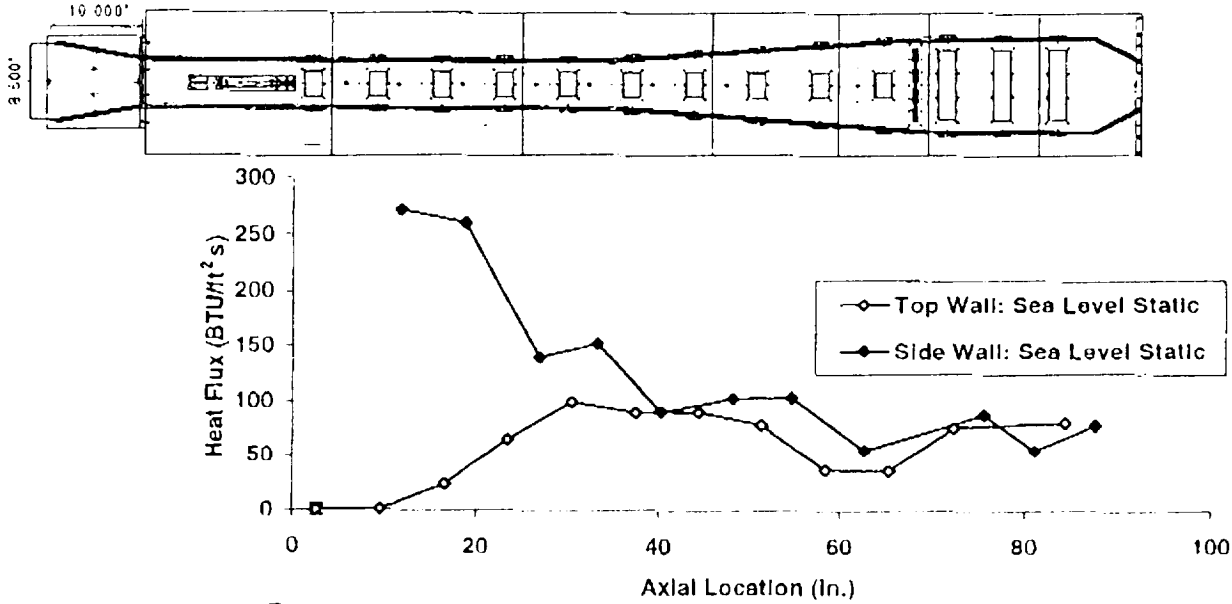

Fig. 8. Wall heat flux profiles for SLS configuration (case 6, Table 1).

The experimental results and the CFD predictions agree qualitatively in terms of overall trends, however, quantitative agreement is not very good.

The wall heat flux profile measurements for case 6 is shown in Fig. 8. Wall heat flux measurements for both the top wall and the side wall are depicted in the figure. Since the rocket exhaust grazes the side walls along the central axis of the rocket-ejector system as it mixes with the cold air from the top and bottom, the highest heat flux levels are measured on the side wall just downstream of the rocket plume. As the rocket exhaust and airstream mix with downstream distance in the mixer the section, the wall heat flux levels for the side and top walls approach each other. Similar qualitative trends were also noted for the remaining cases.

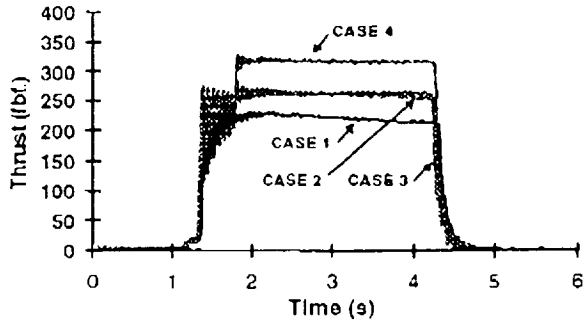

Fig. 9. Thrust versus time traces for all direct-connect cases (cases 1-4, Table 1).

Time traces of the thrust achieved by the engine for all the direct-connect cases (cases 1-4) are shown in Fig. 9. As expected, the measurements show that for both the stoichiometric rocket/afterburner and fuel-rich rocket/no afterburner flow conditions, the thrust level increases with bypass ratio (increased airflow). Also as expected, the thrust results clearly show that for this DAB geometric configuration, the stoichiometric rocket/afterburner flow conditions have higher thrust levels than that of the fuel-rich rocket/no afterburner cases.

The experimental results presented here indicate that for the stoichiometric rocket operation cases, mixing between the rocket exhaust and airstream is near complete within the fourth window location from the rocket nozzle exit plane. In terms of non-dimensional units, mixing is near complete within an axial distance of roughly 39 rocket nozzle exit heights or roughly 5 duct heights. For the fuel-rich rocket cases, the axial distance for near complete mixing and combustion is slightly longer. These measurements in concert with the global measurements of static pressure profiles, wall heat flux profiles and engine thrust provide insight on the fluid dynamic/combustion processes within the rocket-ejector system.

SUMMARY

Raman spectroscopy was applied to study the mixing and combustion characteristics between the rocket exhaust plume and the air stream in an optically-accessible hydrogen/oxygen rocket-ejector system. Experiments were conducted for both direct-connect and SLS configurations for a fixed rocket chamber of 500 psia. Results were obtained for cases where the rocket mixture ratio and overall bypass ratio was varied. These results were complemented by pressure and heat flux measurements to form a complete data set that is being used for anchoring/validating CFD models.

ACKNOWLEDGEMENTS

The authors acknowledge funding from NASA Marshall Space Flight Center under NASA Contract/Grant NAS8-40890. The authors thank Dr. C. L. Merkle for initial development of the DUNS code. The authors also thank Mr. Larry Schaaf fo help in conducting the experiments.

REFERENCES

[1] Escher, W. J. D., ed., The Synerjet Engine: Airbreathing/Rocket Combined-Cycle Propulsion for Tomorrow's Space Transports, Society of Automotive Engineers, Warrendale, PA, 1997.

[2] Billig, F. S., "Advanced Propulsion Technology Program, SSTO Low Speed System Assessment Final Report," The Johns Hopkins University Applied Physics Laboratory, JHU/APL AL-95-A050, June 1995.

[3] Odegaard, E. A. and Stroup, K. E., "1966 Advanced Ramjet Concepts program, Volume VIII-Ejector Ramjet Engine Tests- Phase I" The Marquardt Corporation, Technical Report AFAPL-TR-67-118 Volume VIII, January 1968.

[4] Lehman, M., Pal, S., Broda, J.C. and Santoro, R.J., "Raman Spectroscopy Based Studies of RBCC Ejector Mode Performance," AIAA-99-0090, 37th AIAA Aerospace Sciences Meeting, Reno, NV, January 11-14, 1999.

[5] Lehman, M., Pal, S. and Santoro, R.J., "Experimental Studies of the RBCC Rocket-Ejector Mode," Joint Meeting of the United States Sections: The Combustion Institute, Washington, DC, March 15-17, 1999.

[6] Foust, M. J., Pal, S. and Santoro, R. J., "Gaseous Propellant Rocket Studies using Raman Spectroscopy," AIAA-96-2766 32nd Joint Propulsion Conference, Lake Buena Vista, FL, July 1-3, 1996.

[7] Buelow, P. E. O., Schwer, D. A., Feng, J.-Z., Merkle, C. L. and Choi, D., "A Preconditioned Dual-Time, Diagonalized ADI Scheme for Unsteady Computations," AIAA-97-2101 CP, 13th AIAA Computational Fluid Dynamics Meeting, Snowmass, CO, 1997.

[8] Venkateswaran, S., Buelow, P. E. O. and Merkle, C. L., "Development of Linearized Preconditioning Methods for Enhancing Robustness and Efficiency of Euler and Navier-Stokes Computations," AIAA-97-2039 CP, 13th AIAA Computational Fluid Dynamics Meeting, Snowmass, CO, 1997.

[9] Coakley, T.J., "Turbulence Modeling Methods for the Compressible Navier-Stokes Equations," AIAA-83-1693, AIAA 16th Plasmadynamics Conference, Danvers, MA, 1983.

[10] Briley, W. R. and McDonald, H., "Solution of the Multidimensional Compressible Navier-Stokes Equations by a Generalized Implicit Method," *Journal of Computational Physics*, Vol. 24, 1977, pp. 372-397.

[11] Pulliam, T. H. and Chaussee, D. S., "A Diagonal Form of an Implicit Approximate Factorization Algorith," *Journal of Computational Physics*, Vol. 39, 1981, pp. 347-363.

[12] McBride, B. J. and Gordon, S., Computer Program for Calculation of Complex Chemical Equilibrium Compositions and Applications, NASA Reference Publication 1311, 1996.

[13] Long, D.A., Raman Spectroscopy, McGraw-Hill International Book Company, 1977.

[14] Lederman, S., "The Use of Laser Raman Diagnostics in Flow Fields and Combustion," Prog. Energy Combust. Sci., Vol. 3, 1977, pp. 1-34.

[15] Eckbreth, A. C., Laser Diagnostics for Combustion Temperature and Species. Energy and Engineering Sciences Series, eds A.K. Gupta and D.G. Lilley, Vol. 7, Abacus Press. Cambridge, Massachusetts.

[16] Hassel, E.P., Raman Scattering Experiment Simulator (RAMSES) Version 2.0. Institute fur Energie- und Fraftwerkstechnik, Technische Hochschule, Darmstadt, Germany, 1996.